Published online 14 June 2016

Nucleic Acids Research, 2016, Vol. 44, No. 19 ***6971–6980***
doi: 10.1093/nar/gkw542

Structural and functional characterization of KEOPS dimerization by Pcc1 and its role in t^6A biosynthesis

Leo C.K. Wan[1,2], Monica C. Pillon[3], Neroshan Thevakumaran[1,4], Yulong Sun[5], Avi Chakrabartty[4,5], Alba Guarné[3], Igor Kurinov[6], Daniel Durocher[1,2] and Frank Sicheri[1,2,4,*]

[1]Lunenfeld-Tanenbaum Research Institute, Mount Sinai Hospital, Toronto, ON M5G 1X5, Canada, [2]Department of Molecular Genetics, University of Toronto, Toronto, ON M5S 3E1, Canada, [3]Department of Biochemistry and Biomedical Sciences, McMaster University, Hamilton, ON L8S 4K1, Canada, [4]Department of Biochemistry, University of Toronto, Toronto, ON M5S 1A8, Canada, [5]Department of Medical Biophysics, University of Toronto, Toronto, ON M5S 1L7, Canada and [6]Cornell University, Department of Chemistry and Chemical Biology, NE-CAT, Building 436E, Advanced Photon Source, 9700 S. Cass Avenue, Argonne, IL 60439, USA

Received November 24, 2015; Revised May 27, 2016; Accepted June 3, 2016

ABSTRACT

KEOPS is an ancient protein complex required for the biosynthesis of N6-threonylcarbamoyladenosine (t^6A), a universally conserved tRNA modification found on all ANN-codon recognizing tRNAs. KEOPS consist minimally of four essential subunits, namely the proteins Kae1, Bud32, Cgi121 and Pcc1, with yeast possessing the fifth essential subunit Gon7. Bud32, Cgi121, Pcc1 and Gon7 appear to have evolved to regulate the central t^6A biosynthesis function of Kae1, but their precise function and mechanism of action remains unclear. Pcc1, in particular, binds directly to Kae1 and by virtue of its ability to form dimers in solution and in crystals, Pcc1 was inferred to function as a dimerization module for Kae1 and therefore KEOPS. We now present a 3.4 Å crystal structure of a dimeric Kae1–Pcc1 complex providing direct evidence that Pcc1 can bind and dimerize Kae1. Further biophysical analysis of a complete archaeal KEOPS complex reveals that Pcc1 facilitates KEOPS dimerization *in vitro*. Interestingly, while Pcc1-mediated dimerization of KEOPS is required to support the growth of yeast, it is dispensable for t^6A biosynthesis by archaeal KEOPS *in vitro*, raising the question of how precisely Pcc1-mediated dimerization impacts cellular biology.

INTRODUCTION

Transfer RNAs (tRNAs) are essential adaptor molecules in the protein translation process. They are responsible for providing the correct amino acids for protein translation through decoding the information written in the messenger RNA (mRNA). In order to function at high efficiency and fidelity, all tRNAs are subjected to post-transcriptional modifications (1). These modifications confer both stability and functionality to the tRNA molecule (2). N6-threonylcarbamoylation, which occurs on adenosine 37 of the tRNA anticodon stem loop immediately 3' to the anticodon (3–7), is a universally conserved modification across all branches of life. N6-threonylcarbamoylation occurs on all ANN-recognizing tRNAs with the exception of bacterial initiator $tRNA^{Met}$. In certain species of fungi, plants and bacteria, N6-threonylcarbamoyladenosine (t^6A) can be further processed into cyclic-t^6A (8). The presence of t^6A37 or cyclic-t^6A37 restructures the tRNA anticodon stem loop by preventing A37-U33 hydrogen bonding, which allows t^6A37 to form base-stacking interaction with the mRNA codons. This event strengthens the interaction between the mRNA ANN codon and the tRNA anticodon, thus preventing frameshifting events during translation elongation. It also promotes selection of the cognate starting AUG codon during translation initiation (9,10).

The biosynthesis of t^6A in all branches of life is a two-step process catalyzed sequentially by the Sua5 (in eukaryotes and archaea)/YrdC (in bacteria) and Kae1 (in eukaryotes and archaea)/Qri7 (in mitochondria)/YgjD (in bacteria) protein families (11–13). Sua5/YrdC converts the substrates threonine, adenosine triphosphate (ATP) and bicarbonate into the short-lived small molecule intermediate threonylcarbamoyl-adenylate (TC-AMP) (14,15). TC-AMP is then utilized by the Kae1/Qri7/YgjD protein family for the final formation of t^6A on substrate tRNAs (14,15). Kae1/Qri7/YgjD family members function as a component of related but distinct protein complexes in the three different branches of life. In bacteria, YgjD functions within a ternary complex with the proteins YeaZ (an inactive structural ortholog of YgjD) and YjeE (16–18). In the mitochondria of eukaryotes, Qri7 functions as an isolated homodimer (15,19). In eukaryotes and archaea, Kae1

*To whom correspondence should be addressed. Tel: +1 416 586 8471; Fax: +1 416 586 4800; Email: sicheri@lunenfeld.ca

functions as part of the KEOPS (kinase, endopeptidase and other proteins of small sizes) complex (20–22). In addition to Kae1, KEOPS consists of the adenosine triphosphatase (ATPase) Bud32, the ATPase regulator Cgi121, the dimerization subunit Pcc1 and in fungal species the intrinsically disordered protein Gon7. Atomic structures of archaeal KEOPS sub-complexes support a composite linear architecture consisting of Cgi121-Bud32-Kae1-Pcc1-Pcc1-Kae1-Bud32-Cgi121 (20) while atomic structures of yeast KEOPS sub-complexes support a composite linear architecture consisting of Gon7-Pcc1-Kae1-Bud32-Cgi121 (23). The formation of t^6A is dependent on the integrity of the KEOPS complex as null yeast strains for any KEOPS subunit severely compromises t^6A modification within cells (11,12,15). Intriguingly, yeast cells lacking KEOPS subunits or Sua5 additionally display slow growth and shortened telomere phenotypes (24–26). The underlying mechanistic link between growth, telomere phenotype and t^6A biosynthesis in yeast remains to be determined.

The KEOPS subunits Cgi121, Bud32, Pcc1 and Gon7 (which is currently only found in yeast) have likely evolved to assist or regulate the t^6A biosynthetic function of Kae1. However, the precise molecular function of each subunit remains unclear. In particular, Pcc1 has been proposed to act as a dimerization module for KEOPS based on the following observations. Firstly, *Pyrococcus furiosus* (pfu) Pcc1 in isolation formed homodimers as evidenced by analytical ultracentrifugation and by X-ray crystallography (20). In addition, the symmetrical nature of the homodimer presented two equivalent and non-overlapping surfaces for binding Kae1 and thus could potentially dimerize KEOPS (20). Secondly, the Pcc1 homodimer requires two intact Kae1 binding surfaces to support the growth of yeast. Specifically, a synthetic Pcc1–Pcc1 fusion protein engineered to form homodimers in cis was deficient for the ability to support yeast growth when one or both Kae1 binding surfaces within the synthetic Pcc1–Pcc1 homodimer were disabled by mutation (20). Thirdly, human KEOPS was inferred to form dimers through Pcc1, based on co-immunoprecipitation experiments in HEK293T cells using differentially tagged Kae1 proteins (27).

In contrast, other observations support the possibility that Pcc1 may not function as a dimerization module. Firstly, the crystal structure of an archaeal Kae1–Pcc1 complex revealed a 1:2 stoichiometry, despite the fact that the Pcc1 dimer presented two accessible Kae1 binding surfaces that in principle could accommodate a 2:2 binding stoichiometry (20). Secondly, a recently determined crystal structure of a yeast Pcc1–Gon7 complex revealed a 1:1 stoichiometry in which Pcc1 engaged Gon7 using the same surface previously shown to mediate Pcc1 homodimerization (23). In support of this 1:1 binding mode, which would disrupt the ability of Pcc1 to form homodimers, SEC-MALS analysis of the five-subunit yeast KEOPS complex consisting of Gon7, Pcc1, Kae1, Bud32 and Cgi121 subunits demonstrated a 1:1:1:1:1 binding stoichiometry (23).

Thus, the sum of biological, biochemical and biophysical studies of archaea, yeast and human KEOPS present conflicting pictures of whether Pcc1 functions as a dimerization module within KEOPS. To investigate this issue further, we have now solved and characterized a crystal structure of a *Methanococcus jannaschii* (mj) Kae1–pfuPcc1 complex. The structure revealed the presence of both 1:2 and 2:2 Kae1:Pcc1 binding stoichiometries within the same crystal lattice. Furthermore, SEC-MALS and SAXS analyses revealed that Kae1 and Pcc1 form a 2:2 binding complex in solution highly similar to the configuration displayed in the crystal lattice. Lastly, using a synthetic Pcc1–Pcc1 fusion protein strategy, we characterized the impact of Pcc1-mediated dimerization of KEOPS on the biosynthesis of t^6A in vitro using purified archaeal proteins. These functional studies revealed that perturbation of Pcc1-mediated dimerization of KEOPS had no effect on t^6A biosynthesis activity *in vitro*.

MATERIALS AND METHODS

Plasmid construction, protein expression and purification

pfuPcc1 (full-length) (NCBI accession number WP_011013156.1) and mjKae1 (amino acids 1–328) (NCBI accession number Q58530.2) were amplified from P.furiosus and M.jannaschii genomic DNA (ATCC) respectively using polymerase chain reaction (PCR). PCR products were subcloned using BamHI and XhoI restriction digest sites into a modified pGEX-2T vector (GE Healthcare) harboring the multiple cloning site of pProEx-Hta (ThermoFisher Scientific) and a TEV protease recognition sequence in place of the Thrombin protease recognition sequence. The resulting vector enables expression of TEV cleavable N-terminal glutathione-S-transferase (GST) fusion proteins. Sequence verified plasmids were transformed into *Escherichia coli* BL21 (DE3) CodonPlus cells. Eight-liter cultures were grown at 37°C to an $O.D_{600nm}$ of 0.6–0.8 before induction with 0.3 mM Isopropyl β-D-1-thiogalactopyranoside (IPTG), followed by an overnight growth at 18°C. Bacteria pellets were resuspended and lysed by homogenization in lysis buffer consisting of 50 mM Hepes-HCl pH 7.5, 500 mM NaCl, 5 mM ethylenediaminetetraacetic acid (EDTA) and 1 mM Dithiothreitol (DTT) . Clarified lysates were gravity-flowed over glutathione sepharose resin followed by washing with 20 column volumes (CV) of lysis buffer. Purified proteins bound to the glutathione sepharose resin were eluted by treatment with the TEV-protease. The eluted proteins were finally purified by size exclusion chromatography using a Superdex 200 10/300 GL column (GE Healthcare) equilibrated with 20 mM HEPES pH 7.5, 100 mM NaCl and 2mM DTT.

Crystallization, structure determination and refinement

Crystals of the mjKae1–pfuPcc1 complex were obtained in a sitting crystallization drop, where 200 nl of a 200 μM mjKae1–pfuPcc1–$mjtRNA^{Lys}$ and 2mM AMP mixture was mixed with 200 nl of 0.1 M Sodium Cacodylate pH 6.5 and 1.26 M Ammonium Sulfate. The crystallization drop was equilibrated against a 50-μl mother liquor reservoir of 0.1 M Sodium Cacodylate pH 6.5 and 1.26 M Ammonium Sulfate. Crystals were cryo-protected by quick-soaking in mother liquor containing 20% glycerol prior to flash freezing in liquid nitrogen. A diffraction dataset was collected on a single crystal at the advanced photon source NE-CAT

beamline 24-ID-C. Data reduction and scaling of X-ray diffraction data was performed using the HKL software suite (28). The structure of the Kae1–Pcc1 protein complex was solved by molecular replacement using Pyrococcus abysii Kae1 (PDB ID: 2IVP) and one protomer of pfuPcc1 (PDB ID: 3ENC) as search models in PHASER (29). Refinement was performed using PHENIX (30). The structure has been deposited to the PDB as PDB ID: 5JMV.

Small-angle X-ray analysis

The Kae1–Pcc1 complex was resolved over a 24 ml Superdex-200 (GE Healthcare) gel filtration column. Sample homogeneity was confirmed by dynamic light scattering analysis and solution scattering data was collected on a Rigaku BioSAXS-1000 instrument over a range of protein concentration (11–43 μM). SAXSLab 3.0.0r1 (Rigaku) was used to generate scattering curves. Sample integrity during data collection was confirmed by comparing 10-min exposures collected before and after data collection. The one-dimensional scattering profiles were identical for all protein concentrations. Data quality was assessed by comparing scattering curves over a range of protein concentrations and exposure times using the ATSAS 2.6.0 program suite (31). Radius of gyration and pair-distance distribution functions were determined using Primus and Gnom, respectively (Supplementary Table S3) (32). The highest quality estimate as determined by AutoRg and AutoGNOM was used to select the sample that was processed further. Ten *ab initio* models were independently generated using DAMMIF (33) and clustered based on the normalized spatial discrepancy using DAMCLUST (34). The reported molecular weight was calculated based on the volume of correlation (35). The theoretical scattering curves of the possible 1:2 and 2:2 Kae1:Pcc1 complex were generated and compared to the solution scattering using Crysol (36).

SEC-MALS analysis

SEC-MALS analysis of all protein complexes were conducted using miniDawn TREOS and Optilab T-rEX detectors (Wyatt Technology) coupled to a 1260 Infinity HPLC system (Agilent Technologies). A WTC-030S5 SEC column (Wyatt Technology) was used for protein separation. Chromatography experiments were conducted in 20 mM Hepes pH 7.5, 250 mM NaCl and 1 mM DTT unless otherwise stated. All data analysis was conducted using the ASTRA software (Wyatt Technology).

Sedimentation equilibrium analytical ultracentrifugation

Sedimentation equilibrium analysis of the mjKae1–pfuPcc1 complex was performed with a Beckman ProteomeLab XL-I centrifuge at 20°C. Data was obtained after 38 hours of centrifugation at each speed (indicated below) by monitoring the relative refractive index between the protein sample and the corresponding blank buffer. Concentrations of 1, 0.5 and 0.25 mg/ml were tested in duplicate. The buffer conditions tested were low salt buffer (20 mM Hepes pH 7.5, 100 mM NaCl, 1 mM DTT), original SEC-MALS buffer (20 mM Hepes pH 7.5, 250 mM NaCl, 1 mM DTT), high salt buffer (20 mM Hepes pH 7.5, 500 mM NaCl, 1 mM DTT) and crystallization condition mimic buffer (50 mM Sodium Cacodylate pH 6.5, 630 mM Ammonium Sulfate). Low salt buffer and original SEC-MALS buffer samples were centrifuged at speeds 7800, 8200 and 8800 rpm while high salt buffer and crystallization condition mimic buffer samples were centrifuged at speeds 7500, 8200 and 8800 rpm. Sedimentation equilibrium data was processed using Origin 4.0 software.

HPLC analysis of tRNA composition

In vitro transcribed tRNA was digested and dephosphorylated according to previously described protocols (37). Ribonucleosides were analyzed on a Discovery C18 (15 cm x 4.6 mm, 5 μM) reverse-phase column (Supelco Analytical) equipped with an Ultrasphere ODS guard column (Beckman). Ribonucleosides were separated over a 35-min linear gradient of 98:2–87.5:12.5 (Buffers A and B respectively) at a flow rate of 1.5 ml/min. The compositions of buffers A and B were 250 mM ammonium acetate pH 6.5 and 40% acetonitrile in HPLC-grade water, respectively. All HPLC experiments were performed on a Dionex Ultimate 3000 HPLC Unit (Thermo Scientific) and data analysis was performed using the Chromeleon HPLC software.

In vitro tRNA transcription and purification

Overlap extension PCR was used to generate mj $tRNA^{LYS(AAA)}$ hepatitis delta virus (HDV) ribozyme DNA fragments. The mjtRNA^{Lys}–HDV ribozyme fragment was ligated into pUC19 and linearized with BamHI prior to performing run-off *in vitro* transcription reactions using T7 RNA Polymerase. Transcription reaction conditions were as follows: 100 mM Tris pH 8.0, 4 mM ATP, 4 mM GTP, 4 mM CTP, 4 mM UTP, 10 mM DTT, 1 mM spermidine, 0.1% Triton X-100, 25 mM $MgCl_2$, 30 ug/ml linearized DNA template, 0.2 mg/ml T7 RNA Polymerase, 10 U/ml thermostable inorganic phosphate (NEB) and 200 U/ml RiboLock™ RNase Inhibitor (Thermo Scientific). Transcription reactions were incubated for four hours at 37°C and terminated by the addition of EDTA to a final concentration of 50 mM. RNA was isolated using a conventional phenol–chloroform extraction protocol, followed by isopropanol precipitation and 80% ethanol washes. Air-dried RNA pellets were solubilized in 8M urea and refolded by rapid dilution into nine volumes of 25 mM Bis-Tris pH 6.5, 1 mM $MgCl_2$ and 0.2 mM EDTA. The refolded tRNA was purified on a Source15Q column (GE Healthcare) using the following chromatography conditions: (i) four CV at 20% B and (ii) linear gradient over 25 CV from 20 to 30% B. Solutions A and B are DEPC-treated water and 2 M NaCl prepared in DEPC-treated water respectively. Fractions containing tRNA were pooled and treated with one volume of isopropanol to precipitate RNA. The precipitated RNA was pelleted using centrifugation, washed with 80% ethanol and then air-dried. The RNA pellet was resuspended in 50 mM Tris–Cl pH 8. Prior to use, the tRNA was refolded by (i) boiling at 95°C for 2 min, (ii) flash cooling on ice, (iii) warming to 50°C, (iv) addition of $MgCl_2$ to a final concentration of 2 mM and (v) slow cooling to room temperature.

In vitro t^6A biosynthesis assay

In vitro t^6A biosynthesis assays using archaea proteins were performed in 50 mM Tris–HCl pH 8.0, 150 mM NaCl, 2.5 mM DTT, 0.5 mM threonine, 0.5 mM $NaHCO_3$, 2 mM ATP, 0.25 mM $MnCl_2$, 0.25 mM $MgCl_2$, 2.5 mM spermidine, 0.5 ul TIPP, 5 μM of mjSua5/mjCgi121/mjKae1/mjBud32, 2 μM Pcc1–Pcc1 fusion protein and 50 μM of mjtRNA^{Lys}. Reactions were incubated at 55°C for the indicated time points and stopped by the addition of EDTA to a final concentration of 25 mM. The tRNA was enzymatically digested and analyzed by HPLC as described above.

RMSD calculations

All structure comparisons and RMSD calculations were performed using the SUPERPOSE software (38).

RESULTS

Biophysical analysis of a Kae1–Pcc1 protein complex

Our previous crystal structure analysis of a *Thermoplasma acidophilum* (ta) Kae1–pfuPcc1 protein complex revealed a 1:2 binding stoichiometry (20). This observation was puzzling since the Pcc1 homodimer presented two binding surfaces apparently capable of binding the highly conserved Kae1 protein (see Supplementary Figure S1 for structure based sequence alignment). We surmised that the unexpected binding stoichiometry could be the result of the taKae1–pfuPcc1 complex purification protocol, which involved the addition of pfuPcc1 in large excess over taKae1. To discern if the Pcc1 homodimer has the capacity to bind two Kae1 molecules simultaneously in 2:2 stoichiometry, we conducted size-exclusion chromatography coupled to multi-angle light scattering (SEC-MALS) analysis of a 30 μM mjKae1–pfuPcc1 protein complex. A single migrating species eluted with a mass of 90.7 kDa, which was in close agreement with the predicted mass of 91 kDa for a 2:2 binding stoichiometry (Figure 1). We further validated the 2:2 binding stoichiometry by SEC-MALS analysis of a pfuKae1–pfuPcc1 complex, which eluted as a complex with observed mass of 91.7kDa, nearly identical to the predicted 2:2 mass of 89.5 kDa (Supplementary Figure S2). These observations indicated that under the conditions tested, archaeal Kae1 and Pcc1 proteins bind with 2:2 stoichiometry.

Crystal structure of the 2:2 Kae1–Pcc1 complex

To visualize the atomic details of a 2:2 mjKae1–pfuPcc1 complex, we crystallized an equimolar mixture of mjKae1 with pfuPcc1. Crystals of the mjKae1–pfuPcc1 complex in the presence of the nucleotide AMP were obtained that diffracted to 3.4 Å resolution. The structure was solved by molecular replacement using one protomer of *Pyrococcus abyssi* Kae1 (chain A in PDB ID: 2IVP) and one protomer of pfuPcc1 (chain A in PDB ID: 3ENC) as search models (Table 1). The asymmetric unit consisted of three Kae1 proteins and five Pcc1 proteins, arranged as two complexes with 1:2 binding stoichiometry and one complex with 1:1 stoichiometry (Figure 2A). The configurations with 1:2 stoichiometry were near identical in structure to the previously determined structure of the taKae1–pfuPcc1 complex, with RMSDs ranging from 1.3 Å and 1.5 Å (Supplementary Table S1). Application of crystallographic symmetry to the 1:1 Kae1–Pcc1 complex revealed a higher order arrangement with 2:2 binding stoichiometry (Figure 2B), which we inferred to be the predominant complex detected in solution using SEC-MALS.

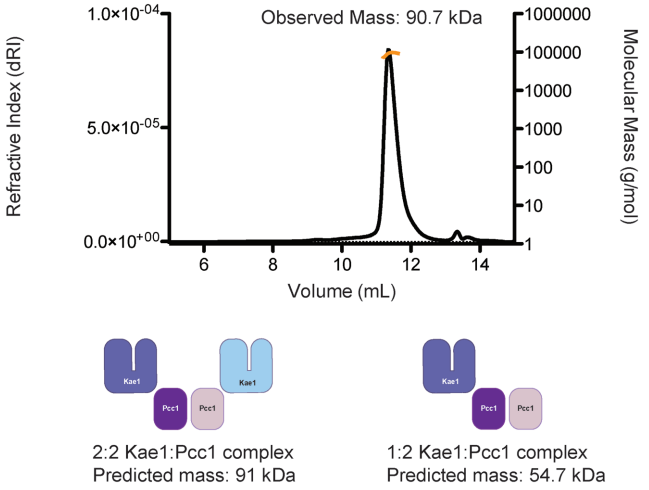

Figure 1. Size exclusion chromatography—multi angle light scattering analysis (SEC-MALS) analysis of a mjKae1–pfuPcc1 complex.

The appearance of both 1:2 and 2:2 Kae1:Pcc1 binding stoichiometries within the same crystal environment suggested that the solution/crystallization conditions could influence subunit assembly. This hypothesis was confirmed by SEC-MALS and sedimentation equilibrium analytical ultracentrifugation (SE-AUC) analyses (Supplementary Figure S3). Both SEC-MALS and SE-AUC analyses of the mjKae1–pfuPcc1 complex performed in an 250 mM NaCl condition revealed comparable apparent molecular masses of 83.6 and 85 kDa respectively, corresponding more closely to the theoretical molecule mass of 91 kDa for a 2:2 binding stoichiometry. In contrast, the same analyses performed in a higher salt condition (500 mM NaCl) revealed comparable apparent molecular masses of 68 and 63 kDa, which is intermediate between 2:2 and 1:2 (55 kDa) binding stoichiometries. Analyses performed in a 100 mM NaCl condition revealed a tendency toward aggregation with an apparent molecular mass of 114 kDa (as evident by a polydispersed peak ranging in size from 85 to 128 kDa) by SEC-MALS and an average molecular mass of 99.5 kDa by SE-AUC. Most notably, SEC-MALS analysis performed in a buffer condition that closely mimicked our crystallization condition (630 mM ammonium sulfate) revealed two distinct complexes with 1:2 and 2:2 binding stoichiometries (65.3 and 85.0 kDa respectively). The appearance of two distinct species rather than a single species likely reflects a slower exchange of binding between Pcc1 and Kae1 in the high ammonium sulfate condition compared to NaCl conditions. SE-AUC analysis in the crystallization mimicking condition revealed an unexpectedly low average molecular mass of 60 kDa. We speculate that this discrepancy with the SEC-MALS measurement may be due to a time de-

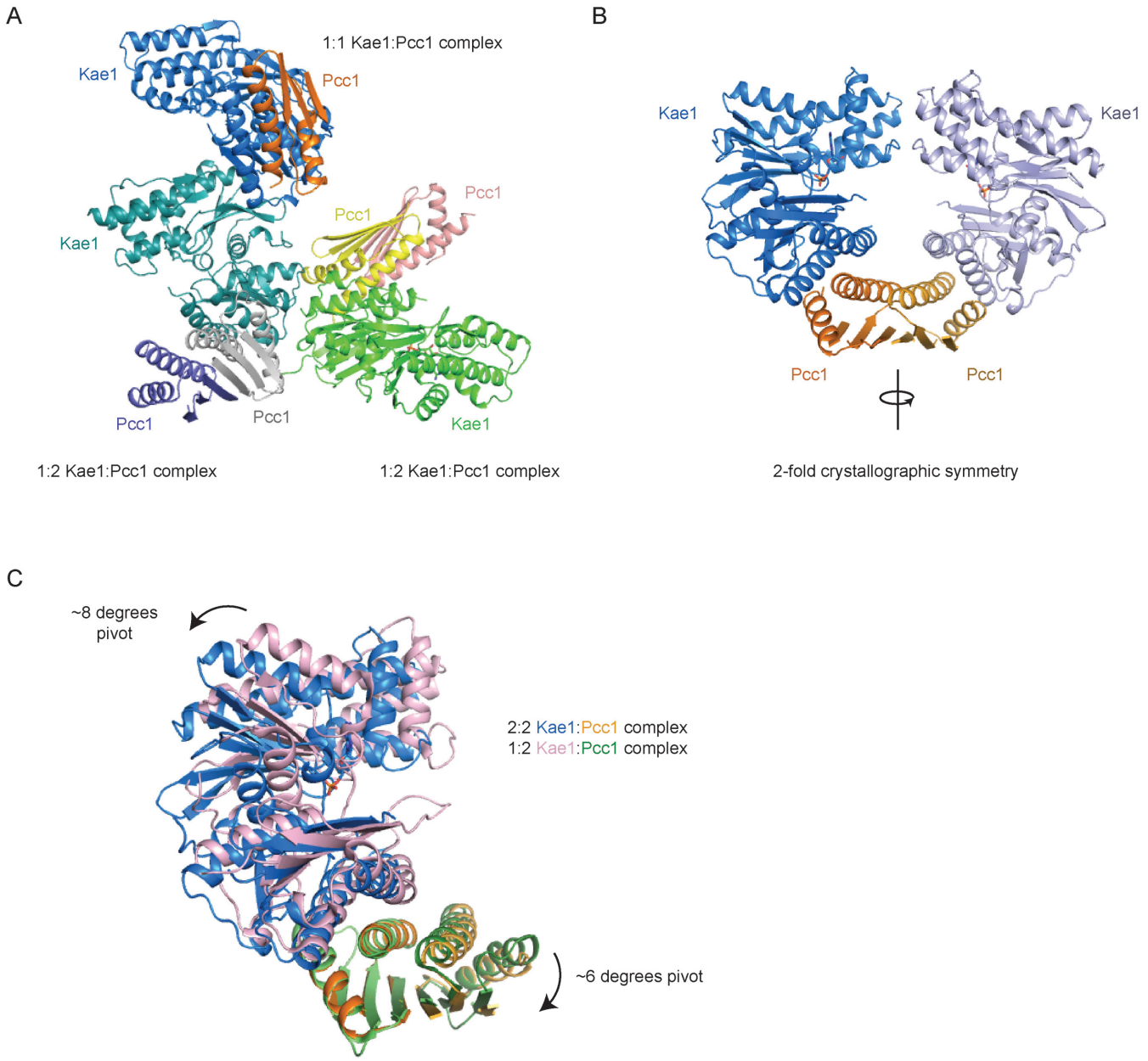

Figure 2. X-ray crystal structure of an archaeal Kae1–Pcc1 protein complex. (**A**) Ribbons representation of the three Kae1 and five Pcc1 proteins in the crystal asymmetrical unit. The eight unique polypeptide chains form two 1:2 Kae1:Pcc1 complexes and one 1:1 Kae1:Pcc1 complex (**B**) Application of crystallographic symmetry to the 1:1 Kae1:Pcc1 complex generates the predicted solution complex with 2:2 stoichiometry. AMP nucleotides are shown in stick representation. (**C**) Comparison of Kae1–Pcc1 complexes with 1:2 and 2:2 stoichiometries. Overlays were performed by superposition of the single central Pcc1 protomer.

pendent instability of the mjKae1–pfuPcc1 complex over the 38-hour SE-AUC experiment. Together these results demonstrated that the binding stoichiometry between Pcc1 and Kae1 is influenced by solution conditions and that the solution conditions employed for crystallization supports the sampling of both 1:2 and 2:2 Kae1–Pcc1 binding stoichiometries in solution, which is in agreement with our observations in the crystal environment.

We previously modeled a 2:2 Kae1–Pcc1 complex using the 1:2 Kae1:Pcc1 structure and observed steric clashes between opposing Kae1 subunits (Supplementary Figure S4). Comparison of the newly determined structure with the predicted 2:2 binding model revealed the basis for how steric hindrance between the two Kae1 protomers is relieved. Firstly, Kae1 protomers are rotated outward by ∼8° about the Kae1–Pcc1 binding surface (Figure 2C). Secondly, each Pcc1 protomer undergoes ∼6° twist about its homodimerization interface (Figure 2C). Beyond these accommodating differences, the structure of the individual Pcc1 and Kae1 protomers are similar across the 1:2 and 2:2 Kae1–Pcc1 complexes observed within the crystal asymmetric unit and across previously determined Kae1 and Pcc1 crystal struc-

Table 1. Data collection and refinement statistics (molecular replacement)

	Kae1–Pcc1 Complex
Data collection	
Space group	$P4_32_12$
Cell dimensions	
a, *b*, *c* (Å)	121.9, 121.9, 310.6
α, β, γ (°)	90, 90, 90
Resolution (Å)	50.0–3.38 (3.52–3.38)[a]
R_{pim}	6.2% (>100%)
CC1/2	0.89 (0.44)
$I / \sigma I$	13.6 (0.94)
Completeness (%)	99.9% (100%)
Redundancy	8.4 (8.1)
Refinement	
Resolution (Å)	48.2–3.38 (3.51–3.38)
No. reflections	28190 (763)
R_{work}/R_{free}	20.0/24.2% (30.9/40.2%)
No. atoms	
Protein	10 321
Ligand/ion	122
B-factors	
Protein	66.0
Ligand/ion	27.8
R.m.s. deviations	
Bond lengths (Å)	0.002
Bond angles (°)	0.72

A single crystal was used for structure determination and 5% of reflections were set aside for R_{free} calculations.
[a]Values in parentheses are for highest-resolution shell.

tures (Complete RMSD analysis in Supplementary Tables S1 and S2).

Small angle X-ray scattering (SAXS) analysis of Kae1–Pcc1

To confirm that the 92 kDa protein complex we observed in solution by SEC-MALS analysis corresponded to the 2:2 Kae1-Pcc1 complex visualized in the newly determined crystal structure, we performed SAXS analyses at three different Kae1–Pcc1 complex concentrations (Supplementary Table S3). Analysis of the scattering curves uniformly revealed an apparent molecular weight of 95.4 kDa, consistent with a 2:2 binding stoichiometry. Comparison of experimental to theoretical scattering profiles for the 2:2 and 1:2 Kae1-Pcc1 structural models using CRYSOL revealed chi^2 values of 1.2 and 5.6 respectively, further supporting that the 2:2 complex visualized in the crystal environment is the same complex sampled in solution (Figure 3A and B). Lastly, *ab initio* modeling revealed a molecular envelope highly similar to the 2:2 Kae1-Pcc1 complex visualized in the crystal lattice (Figure 3C). These observations support the notion that the 2:2 complex visualized in our crystal structure shares the same stoichiometry and configuration sampled in solution.

The KEOPS complex can form super dimers in solution

Since mjKae1 and pfuPcc1 proteins can form 2:2 binding complexes in solution, we hypothesized that the entire KEOPS complex could in turn form super dimers in solution. Indeed, as assessed by SEC-MALS analysis, an equimolar (10 μM) mixture of pfuPcc1, mjKae1, mjBud32 and mjCgi121 recombinant proteins eluted as a single migrating species with a calculated molecular mass of 152.5 kDa, in close agreement with the theoretical molecular mass of 173.4 kDa for a KEOPS super dimer (Figure 4A).

Functional relevance of Pcc1-mediated dimerization of KEOPS on t^6A biosynthesis *invitro*

To probe the functional relevance of Pcc1 mediated dimerization of KEOPS for t^6A biosynthesis *in vitro*, we exploited a synthetic pfuPcc1–Pcc1 fusion protein that enabled selective mutation of one of two Kae1 binding surfaces within the context of a Pcc1 homodimer generated in cis (see Figure 4B for schematic). This strategy to disrupt KEOPS dimerization was necessitated by our previous observation that mutations engineered to disrupt Pcc1 homodimerization directly yielded misfolded proteins (20). We generated three variants of the Pcc1–Pcc1 fusion protein: wild-type–wild-type, wild-type-E30R and wild-type-A75Y/V79R (Figure 4B). Both E30R and A75Y/V79R mutations were shown previously to disrupt pfuPcc1 binding to mjKae1 using a GST pulldown assay (20). Consistent with our design hypothesis, SEC-MALS analysis revealed that KEOPS complexes assembled using the engineered Pcc1–Pcc1 fusion proteins produced complexes of desired stoichiometry (Figure 4C). We next examined the t^6A biosynthetic activity of each assembled KEOPS complex in vitro, at concentrations identical to those examined using SEC-MALS. As demonstrate previously (22), the t^6A biosynthetic function of KEOPS was absolutely dependent on the presence of Pcc1 (Figure 4D). Reactions incorporating the wild type Pcc1–Pcc1 fusion protein resulted in robust t^6A production and this activity was not adversely affected by either the E30R or A75/V79R mutation in one Pcc1 protomer of the Pcc1–Pcc1 fusion protein. Thus, Pcc1-

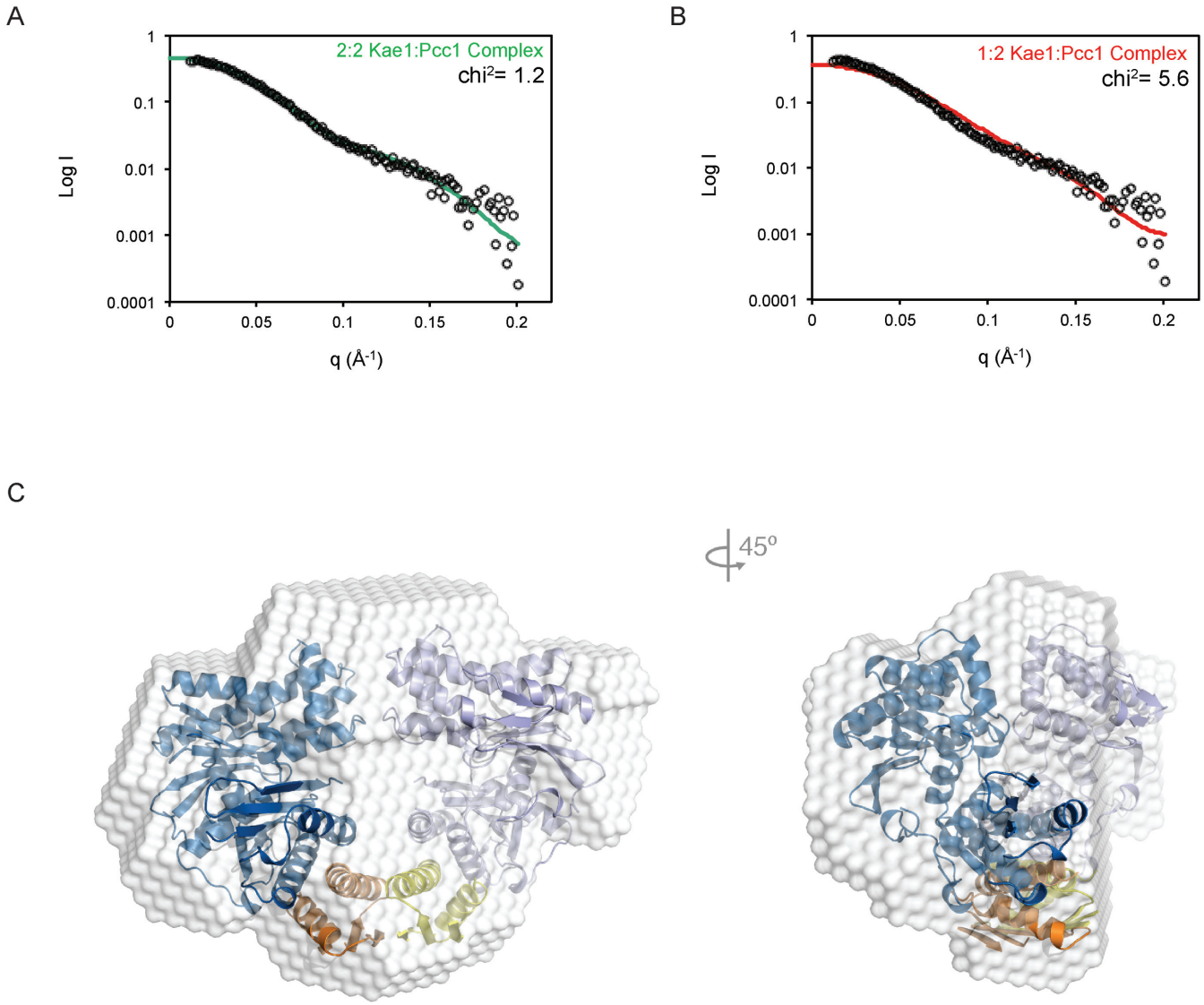

Figure 3. SAXS analysis of the Kae1–Pcc1 complex. (**A**) Crysol comparison of the solution scattering data (black circles) to the theoretical scattering curve (green line) of a 2:2 Kae1-Pcc1 protein structure. (**B**) Crysol comparison of the solution scattering data (black circles) to the theoretical scattering curve (red line) of a 1:2 Kae1-Pcc1 complex. (**C**) Most representative *ab initio* bead model of the Kae1–Pcc1 complex. The crystal structure of the 2:2 Kae1-Pcc1 complex is shown in ribbons representation and manually superimposed onto the bead model for clarity.

mediated dimerization of KEOPS did not appear necessary for t^6A biosynthesis *in vitro,* under the conditions tested.

DISCUSSION

Our studies show that an archaeal KEOPS complex, comprised of mjKae1, pfuPcc1, mjCgi121 and mjBud32 subunits, can form a super dimer *in vitro* facilitated by the ability of Pcc1 to form homodimers and to bind two copies of Kae1. Interestingly, we show that Pcc1 mediated superdimerization of the archaeal KEOPS complex is not essential for t^6A biosynthesis *in vitro*. This contrasts with our previous *in vivo* studies using yeast KEOPS, which indicated that Pcc1-mediated KEOPS dimerization is required to support growth. This may simply reflect the limitation of our *in vitro* reactions to accurately mimic the complexity of the *in vivo* environment. Alternatively, this difference in behavior may reflect evolutionary differences between the archaeal and yeast complexes. Indeed, the two complexes differ in other respects such as in subunit composition with yeast KEOPS containing a fifth subunit, Gon7, that appears absent from archaeal KEOPS.

Functional relevance of divergent modes of dimerization

The ability to form dimeric complexes, either directly or indirectly, is a shared characteristic of all Kae1/Qri7/YgjD family members. Mitochondrial Qri7 forms homodimers directly using the same surface that the bacterial ortholog YgjD heterodimerizes with the inactive structural ortholog YeaZ (15). The homodimerization of Qri7 is required for t^6A biosynthetic function *in vitro* and to support yeast growth *in vivo* (15). While not tested directly by mutagenesis, heterodimerization of YgjD–YeaZ also appears crit-

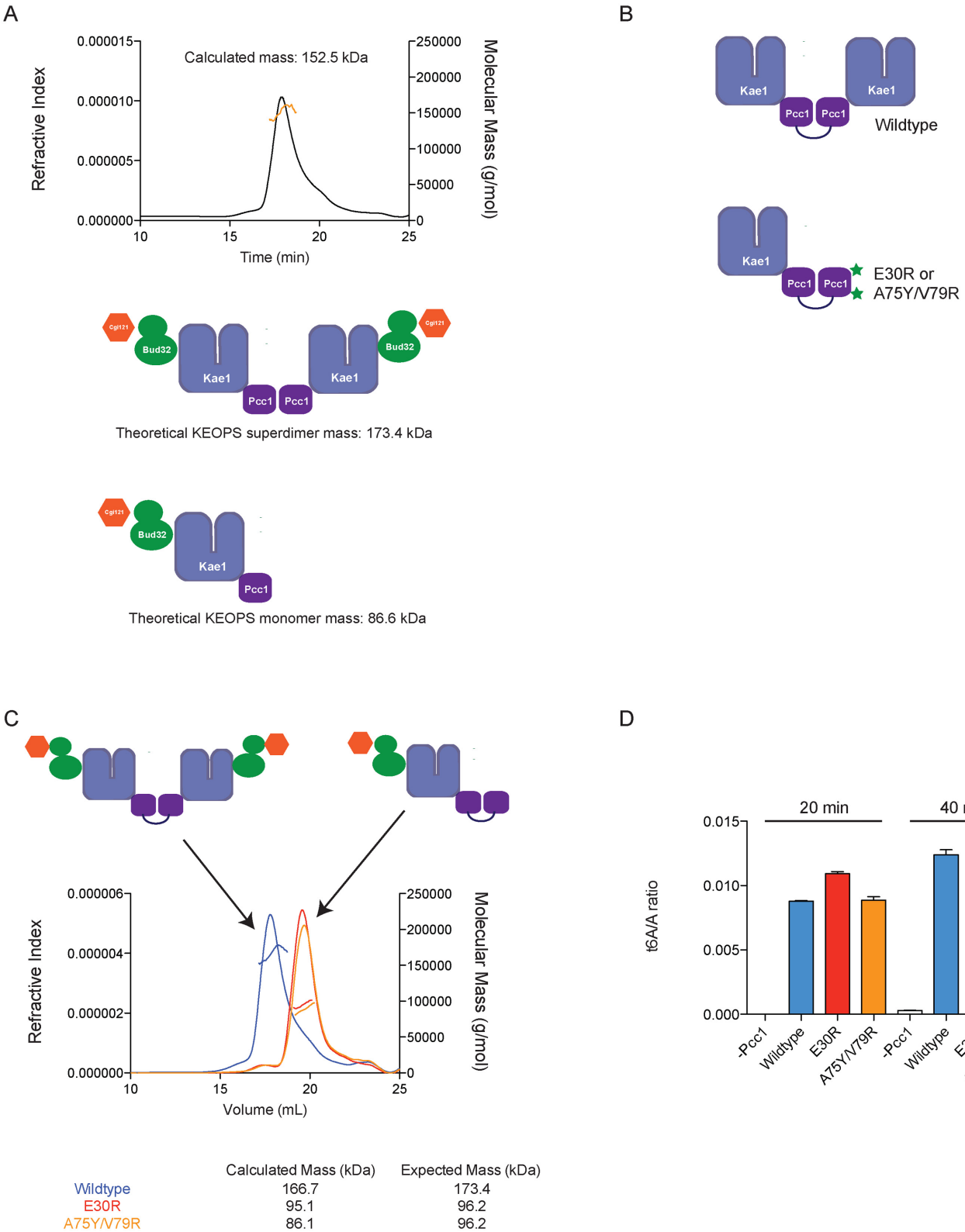

	Calculated Mass (kDa)	Expected Mass (kDa)
Wildtype	166.7	173.4
E30R	95.1	96.2
A75Y/V79R	86.1	96.2

Figure 4. Structure-function characterization of archaea KEOPS *invitro*. (**A**) SEC-MALS elution profile of the archaea KEOPS complex generated using equimolar mixture of pfuPcc1, mjKae1, mjBud32 and mjCgi121 proteins. (**B**) Schematic of pfuPcc1–Pcc1 fusion proteins generated in this study and the predicted binding stoichiometry for Kae1. (**C**) SEC-MALS elution profile for the archaea KEOPS complex incorporating wild-type and mutant pfuPcc1–Pcc1 fusion proteins. (**D**) Analysis of t^6A production by archaea KEOPS complexes incorporating the indicated wild-type or mutant Pcc1–Pcc1 fusion proteins.

ical for growth *in vivo*, as there is a clear obligate dependency between YgjD and YeaZ for their ability to support bacterial growth (11). Perplexingly, eukaryotic and archaeal Kae1 proteins do not appear to dimerize directly either in homotypic fashion or with an inactive structural ortholog. Instead, Kae1 has the potential to dimerize by virtue of binding the dimeric protein Pcc1. Intriguingly, Kae1 uses the same surface to engage Pcc1 that Qri7 and YgjD employ for homo and heterodimerization, respectively. While the contacting secondary structure elements of Pcc1 that binds to Kae1 resemble the corresponding interaction infrastructure in Qri7–Qri7 and YgjD–YeaZ dimers, the end effect of dimerization on the higher order arrangement of Kae1 protomers within KEOPS differs strikingly from the higher order arrangement of Qri7 and YgjD/YeaZ proteins in their dimer states. This dramatic difference in dimer arrangement raises the critical question of what purpose the divergent modes of dimerization serve in the t^6A biosynthetic mechanism.

A compelling model that accounts for the large body of occasionally conflicting observations is that dimerization serves to allosterically regulate the t^6A catalytic function of the Kae1/Qri7/YgjD family. Such a mode of action is exemplified by a subset of eukaryotic protein kinases including the RAF, eIF2α and EGFR kinase families. Members of these three families transition from inactive monomer to active dimer states through direct dimerization of their kinase domains (39–41). Once in their active dimer configurations, each kinase protomer in the dimer is fully self sufficient for phosphotransfer function.

Interestingly, dimer-mediated allosteric regulation of protein kinase function has facilitated the evolution of pseudo enzymes, which maintain the ability to dimerize but have dispensed with the ability to carry out catalysis (42). We speculate that the inactive bacterial ortholog YeaZ evolved in a similar manner, where it maintained the ability to allosterically regulate YgjD through dimerization but dispensed with its own catalytic function. Similarly, dimer mediated allosteric regulation of protein kinases has facilitated the evolution of novel protein interactors that bind the dimerization interface to regulate catalytic output (43). By analogy, we reason that Pcc1 evolved as a novel protein interactor that engages the Kae1 allosteric surface to replace or substitute for the necessity for Kae1 homodimerization. This might explain our observation that while the superdimerization of Kae1 (and by extension KEOPS) mediated by Pcc1 is dispensable for the t^6A catalytic function of archaeal proteins, the presence of Pcc1 in the t^6A biosynthesis reaction is essential. *In vivo* in yeast, the presence of Gon7 adds another layer of complexity to the intra-regulatory system of KEOPS. By virtue of binding to Pcc1 on its homodimerization surface, Gon7 has evolved to regulate the ability of Pcc1 to form homodimers, which by extension, could regulate the dimerization of Kae1 and the larger KEOPS complex (26).

Precisely how the t^6A biosynthesis activity of the Kae1/Qri7/YgjD protein family is regulated by the KEOPS subunits Pcc1, Gon7, Bud32 and Cgi121 and by the bacterial ternary complex subunits YeaZ and YjeE remains a mystery. This is due in great part to our limited understanding of how the Kae1/Qri7/YgjD enzymes binds tRNA and TC-AMP substrates and how they carry out the t^6A catalytic mechanism. High-resolution snapshots of Kae1/Qri7/YgjD in action would provide an invaluable beachhead to unraveling the numerous open mysteries of how the Kae1/Qri7/YgjD family functions.

SUPPLEMENTARY DATA

Supplementary Data are available at NAR Online.

FUNDING

Canadian Institutes of Health Research (CIHR) Foundation Grants [FDN 143277 to F.S., FDN 143343 to D.D.]; CIHR Operating Grant [MOP-67189 to A.G.]; National Institutes of Health [P41 GM103403 to NE-CAT]; NIH-ORIP HEI Grant for Pilatus 6M detector on 24-ID-C beam line [S10 RR029205]; APS funding [DE-AC02-06CH11357]. Funding for open access charge: CIHR Foundation Grant FDN 143277.
Conflict of interest statement. None declared.

REFERENCES

1. El Yacoubi,B., Bailly,M. and de Crecy-Lagard,V. (2012) Biosynthesis and function of posttranscriptional modifications of transfer RNAs. *Annu. Rev. Genet.*, **46**, 69–95.
2. Phizicky,E.M. and Hopper,A.K. (2010) tRNA biology charges to the front. *Genes Dev.*, **24**, 1832–1860.
3. Powers,D.M. and Peterkofsky,A. (1972) The presence of N-(purin-6-ylcarbamoyl)threonine in transfer ribonucleic acid species whose codons begin with adenine. *J. Biol. Chem.*, **247**, 6394–6401.
4. Kimura-Harada,F., Harada,F. and Nishimura,S. (1972) The presence of N-[9-(c-D-ribofuranosyl)purin-6-ylcarbamoyl] threonine in isoleucine, threonine and asparagine tRNAs from Escherichia coli. *FEBS Lett.*, **21**, 71–74.
5. Powers,D.M. and Peterkofsky,A. (1972) Biosynthesis and specific labeling of N-(purin-6-ylcarbamoyl)threonine of Escherichia coli transfer RNA. *Biochem. Biophys. Res. Commun.*, **46**, 831–838.
6. Chheda,G.B., Hong,C.I., Piskorz,C.F. and Harmon,G.A. (1972) Biosynthesis of N-(purin-6-ylcarbamoyl)-L-threonine riboside. Incorporation of L-threonine in vivo into modified nucleoside of transfer ribonucleic acid. *Biochem. J.*, **127**, 515–519.
7. Schweizer,M.P., Chheda,G.B., Baczynskyj,L. and Hall,R.H. (1969) Aminoacyl nucleosides. VII. N-(Purin-6-ylcarbamoyl)threonine. A new component of transfer ribonucleic acid. *Biochemistry*, **8**, 3283–3289.
8. Miyauchi,K., Kimura,S. and Suzuki,T. (2013) A cyclic form of N6-threonylcarbamoyladenosine as a widely distributed tRNA hypermodification. *Nat. Chem. Biol.*, **9**, 105–111.
9. Murphy,F.V.t., Ramakrishnan,V., Malkiewicz,A. and Agris,P.F. (2004) The role of modifications in codon discrimination by tRNA(Lys)UUU. *Nat. Struct. Mol. Biol.*, **11**, 1186–1191.
10. Weissenbach,J. and Grosjean,H. (1981) Effect of threonylcarbamoyl modification (t6A) in yeast tRNA Arg III on codon-anticodon and anticodon-anticodon interactions. A thermodynamic and kinetic evaluation. *Eur. J. Biochem.*, **116**, 207–213.
11. El Yacoubi,B., Hatin,I., Deutsch,C., Kahveci,T., Rousset,J.P., Iwata-Reuyl,D., Murzin,A.G. and de Crecy-Lagard,V. (2011) A role for the universal Kae1/Qri7/YgjD (COG0533) family in tRNA modification. *EMBO J*, **30**, 882–893.
12. Srinivasan,M., Mehta,P., Yu,Y., Prugar,E., Koonin,E.V., Karzai,A.W. and Sternglanz,R. (2011) The highly conserved KEOPS/EKC complex is essential for a universal tRNA modification, t6A. *Embo J.*, **30**, 873–881.
13. El Yacoubi,B., Lyons,B., Cruz,Y., Reddy,R., Nordin,B., Agnelli,F., Williamson,J.R., Schimmel,P., Swairjo,M.A. and de Crecy-Lagard,V. (2009) The universal YrdC/Sua5 family is required for the formation

of threonylcarbamoyladenosine in tRNA. *Nucleic Acids Res.*, **37**, 2894–2909.
14. Lauhon,C.T. (2012) Mechanism of N6-threonylcarbamoyladenonsine (t(6)A) biosynthesis: isolation and characterization of the intermediate threonylcarbamoyl-AMP. *Biochemistry*, **51**, 8950–8963.
15. Wan,L.C., Mao,D.Y., Neculai,D., Strecker,J., Chiovitti,D., Kurinov,I., Poda,G., Thevakumaran,N., Yuan,F., Szilard,R.K. *et al.* (2013) Reconstitution and characterization of eukaryotic N6-threonylcarbamoylation of tRNA using a minimal enzyme system. *Nucleic Acids Res.*, **41**, 6332–6346.
16. Nichols,C.E., Lamb,H.K., Thompson,P., Omari,K.E., Lockyer,M., Charles,I., Hawkins,A.R. and Stammers,D.K. (2013) Crystal structure of the dimer of two essential Salmonella typhimurium proteins, YgjD & YeaZ and calorimetric evidence for the formation of a ternary YgjD-YeaZ-YjeE complex. *Protein Sci.*, **22**, 628–640.
17. Handford,J.I., Ize,B., Buchanan,G., Butland,G.P., Greenblatt,J., Emili,A. and Palmer,T. (2009) Conserved network of proteins essential for bacterial viability. *J. Bacteriol.*, **191**, 4732–4749.
18. Deutsch,C., El Yacoubi,B., de Crecy-Lagard,V. and Iwata-Reuyl,D. (2012) Biosynthesis of threonylcarbamoyl adenosine (t6A), a universal tRNA nucleoside. *J. Biol. Chem.*, **287**, 13666–13673.
19. Oberto,J., Breuil,N., Hecker,A., Farina,F., Brochier-Armanet,C., Culetto,E. and Forterre,P. (2009) Qri7/OSGEPL, the mitochondrial version of the universal Kae1/YgjD protein, is essential for mitochondrial genome maintenance. *Nucleic Acids Res.*, **37**, 5343–5352.
20. Mao,D.Y., Neculai,D., Downey,M., Orlicky,S., Haffani,Y.Z., Ceccarelli,D.F., Ho,J.S., Szilard,R.K., Zhang,W., Ho,C.S. *et al.* (2008) Atomic structure of the KEOPS complex: an ancient protein kinase-containing molecular machine. *Mol. Cell*, **32**, 259–275.
21. Kisseleva-Romanova,E., Lopreiato,R., Baudin-Baillieu,A., Rousselle,J.C., Ilan,L., Hofmann,K., Namane,A., Mann,C. and Libri,D. (2006) Yeast homolog of a cancer-testis antigen defines a new transcription complex. *EMBO J.*, **25**, 3576–3585.
22. Perrochia,L., Crozat,E., Hecker,A., Zhang,W., Bareille,J., Collinet,B., van Tilbeurgh,H., Forterre,P. and Basta,T. (2012) In vitro biosynthesis of a universal t6A tRNA modification in Archaea and Eukarya. *Nucleic Acids Res.*, **41**, 1953–1964.
23. Zhang,W., Collinet,B., Graille,M., Daugeron,M.C., Lazar,N., Libri,D., Durand,D. and van Tilbeurgh,H. (2015) Crystal structures of the Gon7/Pcc1 and Bud32/Cgi121 complexes provide a model for the complete yeast KEOPS complex. *Nucleic Acids Res.*, **43**, 3358–3372.
24. Downey,M., Houlsworth,R., Maringele,L., Rollie,A., Brehme,M., Galicia,S., Guillard,S., Partington,M., Zubko,M.K., Krogan,N.J. *et al.* (2006) A genome-wide screen identifies the evolutionarily conserved KEOPS complex as a telomere regulator. *Cell*, **124**, 1155–1168.
25. Meng,F.L., Chen,X.F., Hu,Y., Tang,H.B., Dang,W. and Zhou,J.Q. (2010) Sua5p is required for telomere recombination in Saccharomyces cerevisiae. *Cell Res.*, **20**, 495–498.
26. Meng,F.L., Hu,Y., Shen,N., Tong,X.J., Wang,J., Ding,J. and Zhou,J.Q. (2009) Sua5p a single-stranded telomeric DNA-binding protein facilitates telomere replication. *EMBO J.*, **28**, 1466–1478.
27. Costessi,A., Mahrour,N., Sharma,V., Stunnenberg,R., Stoel,M.A., Tijchon,E., Conaway,J.W., Conaway,R.C. and Stunnenberg,H.G. (2012) The human EKC/KEOPS complex is recruited to Cullin2 ubiquitin ligases by the human tumour antigen PRAME. *PLoS One*, **7**, e42822.
28. Minor,W., Cymborowski,M., Otwinowski,Z. and Chruszcz,M. (2006) HKL-3000: the integration of data reduction and structure solution–from diffraction images to an initial model in minutes. *Acta Crystallogr. D Biol. Crystallogr.*, **62**, 859–866.
29. McCoy,A.J., Grosse-Kunstleve,R.W., Adams,P.D., Winn,M.D., Storoni,L.C. and Read,R.J. (2007) Phaser crystallographic software. *J. Appl. Crystallogr.*, **40**, 658–674.
30. Adams,P.D., Afonine,P.V., Bunkoczi,G., Chen,V.B., Davis,I.W., Echols,N., Headd,J.J., Hung,L.W., Kapral,G.J., Grosse-Kunstleve,R.W. *et al.* (2010) PHENIX: a comprehensive Python-based system for macromolecular structure solution. *Acta Crystallogr. D Biol. Crystallogr.*, **66**, 213–221.
31. Petoukhov,M.V., Franke,D., Shkumatov,A.V., Tria,G., Kikhney,A.G., Gajda,M., Gorba,C., Mertens,H.D., Konarev,P.V. and Svergun,D.I. (2012) New developments in the program package for small-angle scattering data analysis. *J. Appl. Crystallogr.*, **45**, 342–350.
32. Konarev,P.V., Volkov,V.V., Sokolova,A.V., Koch,M.H.J. and Svergun,D.I. (2003) PRIMUS: a Windows PC-based system for small-angle scattering data analysis. *J. Appl. Crystallogr.*, **36**, 1277–1282.
33. Svergun,D.F.a.D.I. (2009) DAMMIF, a program for rapid ab-initio shape determination in small-angle scattering. *J. Appl. Crystallogr.*, **42**, 342–346.
34. Petoukhov,M.V., Franke,D., Shkumatov,A.V., Tria,G., Kikhney,A.G., Gajda,M., Gorba,C., Mertens,H.D.T., Konarev,P.V. and Svergun,D.I. (2012) New developments in the ATSAS program package for small-angle scattering data analysis. *J. Appl. Crystallogr.*, **45**, 342–350.
35. Rambo,R.P. and Tainer,J.A. (2013) Accurate assessment of mass, models and resolution by small-angle scattering. *Nature*, **496**, 477–481.
36. Svergun,D., Barberato,C. and Koch,M.H.J. (1995) CRYSOL—a program to evaluate x-ray solution scattering of biological macromolecules from atomic coordinates. *J. Appl. Crystallogr.*, **28**, 768–773.
37. Gehrke,C.W. and Kuo,K.C. (1989) Ribonucleoside analysis by reversed-phase high-performance liquid chromatography. *J. Chromatogr.*, **471**, 3–36.
38. Krissinel,E. and Henrick,K. (2004) Secondary-structure matching (SSM), a new tool for fast protein structure alignment in three dimensions. *Acta Crystallogr. D Biol. Crystallogr.*, **60**, 2256–2268.
39. Dar,A.C., Dever,T.E. and Sicheri,F. (2005) Higher-order substrate recognition of eIF2alpha by the RNA-dependent protein kinase PKR. *Cell*, **122**, 887–900.
40. Rajakulendran,T., Sahmi,M., Lefrancois,M., Sicheri,F. and Therrien,M. (2009) A dimerization-dependent mechanism drives RAF catalytic activation. *Nature*, **461**, 542–545.
41. Zhang,X., Gureasko,J., Shen,K., Cole,P.A. and Kuriyan,J. (2006) An allosteric mechanism for activation of the kinase domain of epidermal growth factor receptor. *Cell*, **125**, 1137–1149.
42. Zeqiraj,E. and van Aalten,D.M. (2010) Pseudokinases-remnants of evolution or key allosteric regulators? *Curr. Opin. Struct. Biol.*, **20**, 772–781.
43. Zhang,X., Pickin,K.A., Bose,R., Jura,N., Cole,P.A. and Kuriyan,J. (2007) Inhibition of the EGF receptor by binding of MIG6 to an activating kinase domain interface. *Nature*, **450**, 741–744.